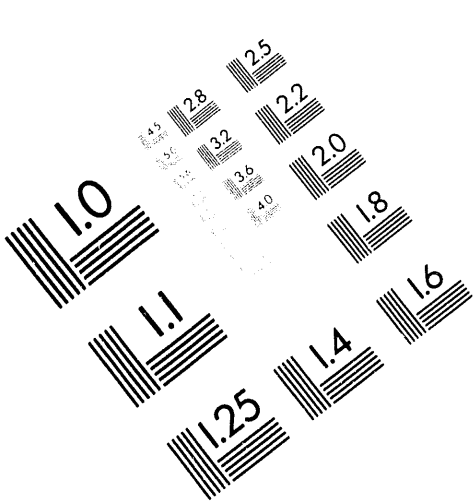

Association for Information and Image Management

1100 Wayne Avenue, Suite 1100
Silver Spring, Maryland 20910

301/587-8202

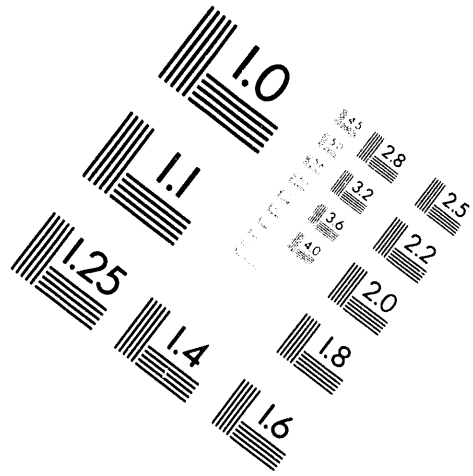

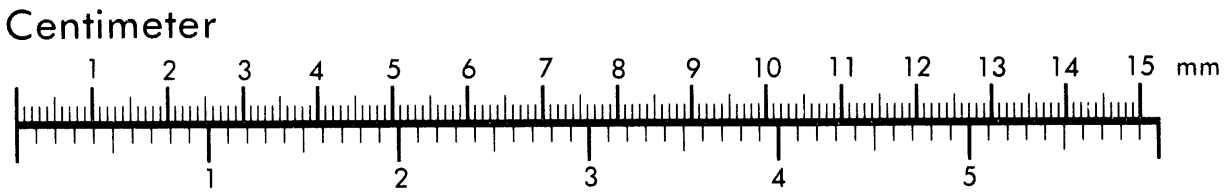

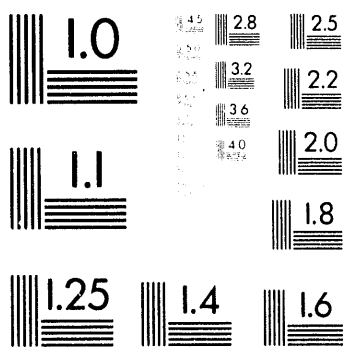

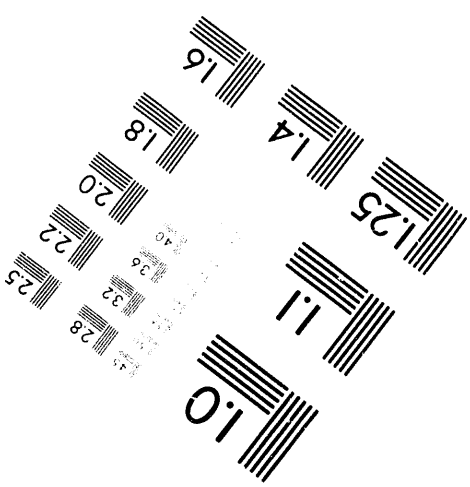

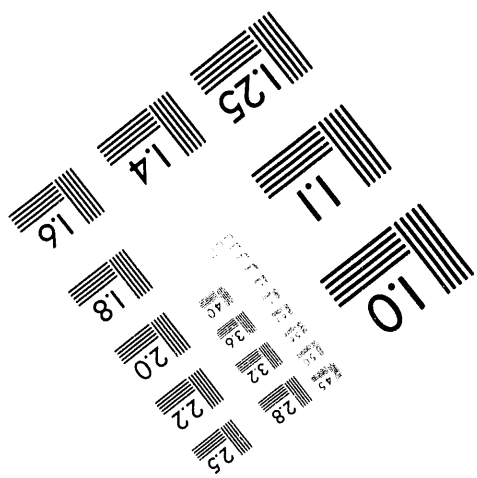

MANUFACTURED TO AIIM STANDARDS
BY APPLIED IMAGE, INC.

1 of 1

Conf-9404100--8

UCRL-JC-116428
PREPRINT

THE INFLUENCE OF MATERIAL MODELS ON CHEMICAL OR NUCLEAR-EXPLOSION SOURCE FUNCTIONS

Lewis A. Glenn
P. Goldstein
Lawrence Livermore National Laboratory

This paper was prepared for submittal to the
DOE Symposium on the Non-Proliferation Experiment Results and Implications for Test Ban Treaties
Rockville, MD
April 19–21, 1994

April 1994

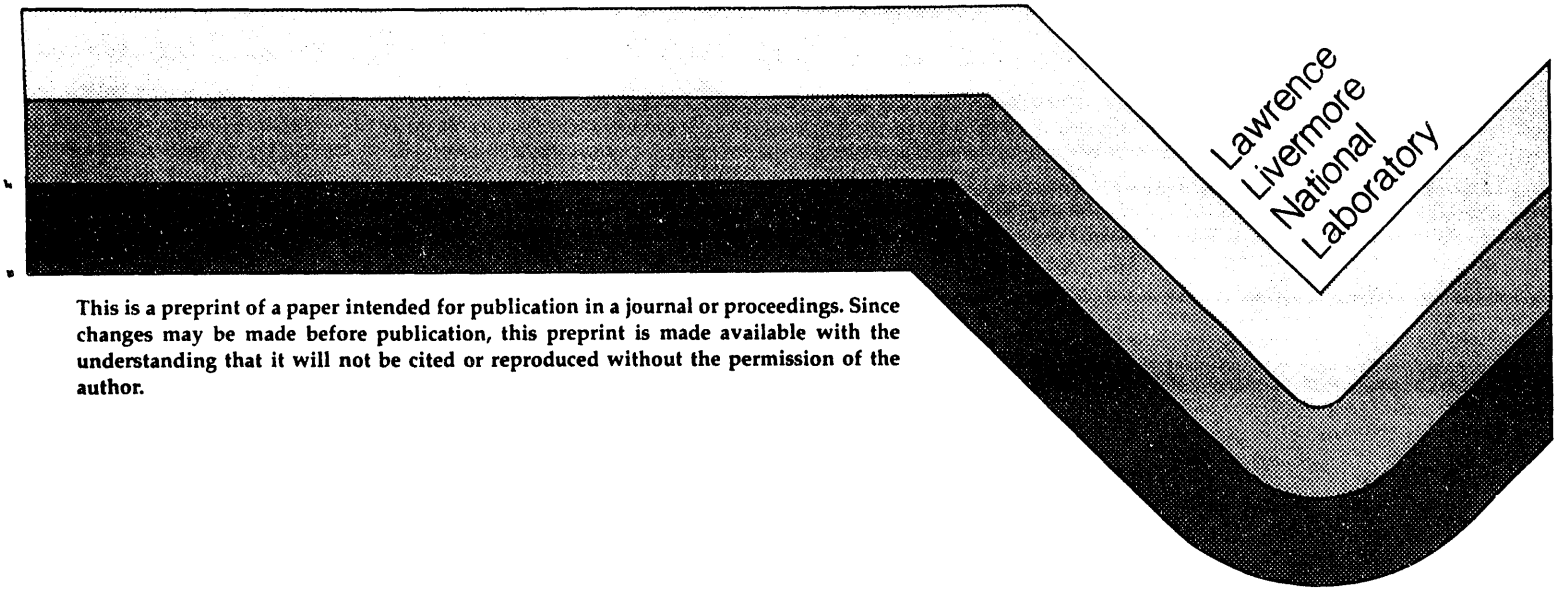

THE INFLUENCE OF MATERIAL MODELS ON CHEMICAL OR NUCLEAR-EXPLOSION SOURCE FUNCTIONS *

L. A. Glenn
P. Goldstein
University of California
Lawrence Livermore National Laboratory
prepared for submittal to:
DOE Symposium on the Non-Proliferation Experiment Results and Implication for Test Ban Treaties

ABSTRACT

Physical models of explosion sources are needed to explain the variations in the performance of existing discriminants in different regions, and to help develop more robust methods for identifying underground explosions.

In this paper, we assess the sensitivity of explosion source functions to material properties by means of numerical simulations. Specifically, we have calculated the effect of varying the yield strength, overburden pressure, and gas porosity on the spectra of the reduced velocity potential for both nuclear and chemical explosions, and compared these with experimental results derived from free-field particle acceleration and regional seismic (LNN) data. The chemical-explosion calculations were intended to simulate the kiloton experiment recently conducted in Area 12 of the Nevada Test Site (NTS) that has been dubbed the Non-Proliferation Experiment (NPE).

We found that the asymptotic (long period) value of the reduced displacement potential, ϕ_∞, for explosions with the ANFO blasting agent used in the NPE, was larger than that derived for a tamped nuclear explosion of the same yield by a factor of 1.9, in good agreement with the experimental results derived from free-field particle velocity measurements, and also with $m_b(P_n)$ data from the Livermore Nevada Network (LNN). Beyond the corner frequency, the spectra calculated for the chemical and nuclear explosions were indistinguishable, also in good agreement with experiment. It was found possible to match the spectral characteristics by varying both the yield strength and the gas porosity, but the strength required to obtain this match was considerably less than measured in laboratory experiments with small cores pulled from the vicinity of the emplacement. Previous experience, however, is that laboratory measurements on core-sized rock samples may not be representative of the extant rock mass from which the samples derive.

* Work performed under the auspices of the U. S. Department of Energy by Lawrence Livermore National Laboratory under contract #W-7405-Eng-48

LNN DATA

Chemical and nuclear explosives are fundamentally different in at least two ways: 1) the energy density is initially much higher with nuclear explosives, and 2) the pressure (at the same energy density) is significantly higher with chemical explosives. Both of these properties are responsible for the higher predicted value of ϕ_∞ when concentrated chemical explosives are substituted for nuclear explosives of the same yield (Glenn, 1993; Glenn and Goldstein; 1994). Figure 1 shows the seismic amplitude as a function of scaled (initial emplacement) cavity radius, as derived from the LNN; note that the abscissa, $r_0 W^{-1/3}$, is the inverse cube root of the initial energy density and the ordinate is effectively the yield-scaled seismic amplitude. The points numbered 1-18 derive from nuclear explosions nearby the site of the NPE, where number 1 was the closest and number 18 the furthest from the NPE site, all within a radius of 2 km. It is observed that most of the nuclear explosions had $r_0 W^{-1/3} \approx 1$ m/kt$^{1/3}$, whereas for the ANFO-emulsion blend employed in the NPE, $r_0 W^{-1/3}$ was ≈ 6 m/kt$^{1/3}$. It is also seen that the yield-scaled seismic amplitude measured in the NPE was roughly twice that of most of the nuclear explosions. Our simulations, discussed below, found a factor of 1.9 when the explosive employed was the ANFO-emulsion mix used for the NPE; with TNT, the factor was approximately 1.6, and in neither case was there any significant dependence on the properties of the surrounding rock. Different explosives produce slightly different results because the effective ratio of specific heats of the explosion products, γ_{eff}, varies with the chemical makeup of the explosive and the cavity pressure is directly proportional to the quantity $(\gamma_{eff} - 1)$.

FREE-FIELD DATA

Figure 2 plots the yield-scaled magnitude of the reduced velocity potential-spectrum, $|i\omega\hat{\phi}|/W$, as a function of yield-scaled frequency, $fW^{1/3}$, where $f = \omega/2\pi$. The heavy black curve is the lognormal average derived from LANL free-field particle acceleration measurements on the NPE and the heavy gray curve plots similar data from a nearby nuclear event; both sets of free-field measurements were provided by F. App of LANL. The dotted curves represent ± 1 standard deviation from the mean. For the nuclear event, 4 gages were employed to calculate $|i\omega\hat{\phi}|/W$. These were all located at ranges beyond 257 m/kt$^{1/3}$; data from gages closer to the explosion were available, but these were found to be within the inelastic region and were therefore excluded for purposes of seismic analysis. We note that the calculation of $\phi(t)$ from the particle acceleration records, $\dot{u}(t)$, required truncation of the records to exclude non-spherical motion in the coda; guidance for the location of the truncation point was provided by reference to the simulations, discussed below. For the NPE results shown in Figure 2, 12 gages were used, all beyond 284 m/kt$^{1/3}$.

At $fW^{1/3}$= 1 Hz-kt$^{1/3}$, the lognormal average value of $|i\omega\hat{\phi}|/W$ for the NPE was found to be 1583 m^3/kt-s-Hz, compared with 819 m^3/kt-s-Hz for the nearby nuclear event; the amplitude ratio is 1.93. Figure 2 shows that beyond 4 Hz-kt$^{1/3}$, however, the average amplitude spectra are virtually indistinguishable.

In what follows, we have attempted to reproduce these results via direct simulation. The computer code employed has been described elsewhere (Glenn, 1978; 1993). Our proceedure was to compare calculations with the nuclear-explosion data and to vary the important elements of the material model for the surrounding rock until an adequate representation was achieved; then, without changing the rock properties, we substituted the ANFO-emulsion blasting agent for the nuclear-explosion source and compared the computed sesimic response with the results of the NPE.

MATERIAL MODELS

The most important elements of the rock model are the strength and gas porosity. Our constitutive model for the nearly saturated tuff employed a tabular equation of state that was fitted to previously obtained shock Hugoniot and elastic-wave data. The shock-wave data are relatively insensitive to small-scale inhomogeneities so that it is generally possible to determine the high-pressure properties of the rock quite accurately. The elastic moduli are also known accurately via wave speed measurements. By contrast, it is difficult to obtain unambiguous strength or porosity data due mainly to the spatial inhomogeneities inherent at most sites.

In our model, the compressive strength of tuff depends on the pressure, temperature, and on a *damage* parameter that measures the degree of degradation due to tensile fracture. Specifically,

$$\sqrt{3J_2'} \le Y = (1-D)\tilde{Y} + \beta D\tilde{Y} \tag{1}$$

where $J_2' \equiv \frac{1}{2}\sigma_{ij}'\sigma_{ij}'$, σ' is the deviatoric stress tensor, β is a constant, typically 0.25, and D is a scalar function of the volumetric component of the void strain tensor (Rubin and Attia, 1990). For this study, $D = \epsilon_{ii}^V/\epsilon_{max}^V$ and ϵ_{max}^V was taken as 5×10^{-3}. Also,

$$\tilde{Y} = \left[Y_0 + \frac{p}{a + (\frac{p}{Y_u - Y_0})} \right] \max\{(1 - T/T_m)^b, 0\} \tag{2}$$

Y_0 is the unconfined compressive strength, Y_u is the ultimate compressive strength, T is temperature, and $T_m(p)$ is the melting point. Here, the cohesion parameter, a was taken as 1.35 and the parameter b was assumed equal to unity.

The equation of state is based on the well-known $p - \alpha$ concept developed by Carroll

and Holt (1972), i.e.,

$$p(v,e) = p_m(v/\alpha, e)/\alpha = p_m(v_m, e_m)/\alpha \tag{3}$$

and

$$\alpha = \alpha(p) \tag{4}$$

where $v = 1/\rho$ is the specific volume, and the subscript $_m$ refers to the matrix material in which the pores are embedded. The parameter α is related to the gas porosity, Ψ, and is defined by the relation

$$\alpha \equiv v/v_m = \rho_m/\rho = (1 - \Psi)^{-1} \tag{5}$$

At ambient pressure, $\alpha = \alpha^0$, the initial value, and at some high pressure, p_c,the pores will be completely crushed and $\alpha(p_c) = 1$. For $p > p_c$, the Grüneisen form, p_m, employed in equation (3) smoothly transitions into the tabular form $p_m(\rho, T)$.

Equations (3) and (4) apply to loading for $p < p_c$, but to unloading only when $p < p_{el}$; in this small, but important, range the pore volume behaves in strictly elastic fashion. In the range $p_{el} \leq p < p_c$, unloading occurs at constant gas porosity.

SIMULATIONS

Figure 3 exhibits calculations of the tamped nuclear explosion where the ultimate yield strength, Y_u, has been varied from 5 MPa to 205 MPa. The gas porosity, Ψ was set to 0 and the overburden pressure, p_{ovb} to 4 MPa; all other parameters were fixed as well. It is observed that the corner frequency decreases significantly with decreasing strength and that the curve derived from the free-field experiments is best matched with the lowest strength.

The nominal overburden pressure for the NPE was roughly 8 MPa. Figure 4 shows the effect of varying p_{ovb} while keeping all other parameters fixed; in this case we have Y_u = 65 MPa, more nearly the nominal value derived from laboratory analysis (Patch *et al.*, 1994), and $\Psi = 0$. It is seen in the figure that the corner frequency is little affected with $2 \leq p_{ovb} \leq 16$ MPa.

Although the simulation with $Y_u = 5$ MPa gives a good fit to the corner frequency, figure 3 shows that the low-frequency (1 Hz-kt$^{1/3}$) amplitude is too high in this case, a situation that can be remedied by increasing the gas porosity; we note that the geological data for the N-tunnel region exhibits significant variations in the measured gas porosity, with the typical range being $0 < \Psi < 0.05$. Figure 5 displays the results of simulations with the gas porosity fixed at 1% ($\Psi = 0.01$) and the overburden pressure fixed at the nominal 8 MPa. Again, we find the calculation with $Y_u = 5$ Mpa gives a good match to the experimental spectra, and this time the low-frequency amplitude is below that

derived from the free-field data. We note in passing that whenever $p_{ovb} > 2Y/3$, as is the case here, the region around the source excavation cannot be in a fully elastic state *prior to the explosion.* This, however, does not preclude mechanical equilibrium from being established, as was demonstrated, for example, by Wells (1969).

Figure 6 shows the effect of further increase in gas porosity. No significant effect on corner frequency is noted but, for example, with $\Psi = 0.05$ both the low- and high-frequency amplitudes are substantially below the experimental data. A quite good fit to the experiment is observed for $0 < \Psi < 0.01$. The simulations with $\Psi = 0.01$ and 0.02 are practically congruent below the corner frequency, although the $\Psi = 0.02$ simulation evidences a slight overshoot and falls significantly below the experimental data at frequencies above 10 Hz-kt$^{1/3}$.

Figure 7 exhibits simulations of the NPE, with the same parameters that provided the best fit to the nearby nuclear event, i.e., $Y_u = 5$ MPa, $0 < \Psi < 0.01$, and $p_{ovb} = 8$ MPa. These calculations differ from those in figure 6 only in that the ANFO-emulsion blasting agent was substituted for the nuclear device; a JWL equation-of-state was employed for the blasting agent, with the parameters derived from analysis via the TIGER code (Souers and Larson, 1994). Figure 7 shows that the simulations are in equally good agreement with the NPE; in this case the 1%-porosity calculation is closer to the experiment than in the nuclear case.

Finally, the comparison of the peak particle velocities derived via the simulations with those measured is shown in figure 8. Most of the experimental data fall in between the simulations with 0 and 1%-gas porosity. For the NPE, and beyond a range of 400-500 m/kt$^{1/3}$, the data fall somewhat below the 1%-calculation. A slightly higher gas porosity would certainly account for these data, and is by no means excluded based on the geological characteristics of the N-tunnel explosion site.

CONCLUDING REMARKS

The most important elements in simulating the seismic response to underground explosions are the representation of material strength and gas porosity. Other factors such as the high-pressure equation-of-state, elastic moduli, and the overburden state contribute to the result, but strength and porosity are the main determinants of long-period amplitude and corner frequency is mainly set by the strength. We found that it was possible to get a reasonably good match to seismic spectra from both the NPE and a nearby nuclear event with the same material model. However, the strength that provided the match was roughly an order of magnitude less than that determined via laboratory analysis of core samples taken from the vicinity of the test site. This is not an unusual occurrence and derives from the fact that the rock media in which the testing takes place are generally quite inhomogeneous, so that laboratory measurements

on core-sized rock samples may not be representative of the extant rock mass from which the samples derive. We note that this is an inherent limitation in employing simulations to the monitoring function, i.e., simulation of explosions at unidentified (clandestine) locations implies an imperfect knowledge of the *in situ* material properties and emplacement geometry.

REFERENCES

Carroll, M. M. and A. C. Holt. Suggested modification of the p-α model for porous materials, *J. Appl. Phys.*, 43, No. 2, 759-761, 1972.

Glenn, L. A. AFTON Revisited: An improved algorithm for numerical solution of initial value problems in continuum mechanics; part 1, the one-dimensional equations, Lawrence Livermore National Laboratory Report, Livermore CA, UCRL-52512, 1978.

Glenn, L. A. Energy-density effects on seismic decoupling, *J. Geophys. Res.*, 98, B2, 1933-1942, 1993.

Glenn, L. A. and P. Goldstein. Seismic decoupling with chemical and nuclear explosions in salt, *J. Geophys. Res.*, in press; see also University of California, Lawrence Livermore National Laboratory Preprint UCRL-JC-114711, August 1993.

Patch, D. F., Welch, J. E. and J. Zerkle. Preshot predictions for the Near-Source Region in the NPE, this symposium.

Rubin, M. B. and A. V. Attia. A continuum tensile failure model with friction, University of California, Lawrence Livermore National Laboratory Report UCRL-ID-104759, August 21, 1990.

Souers, P. C. and D. B. Larson. TIGER calculations and the NPE energy yield, this symposium.

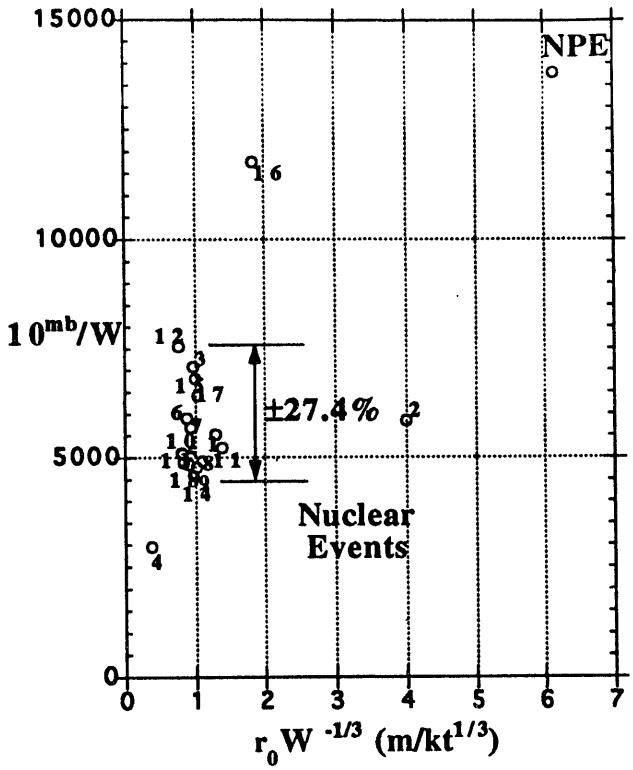

Fig. 1 Seismic amplitude as a function of initial emplacement radius. Numbers refer to location of nuclear events relative to the NPE.

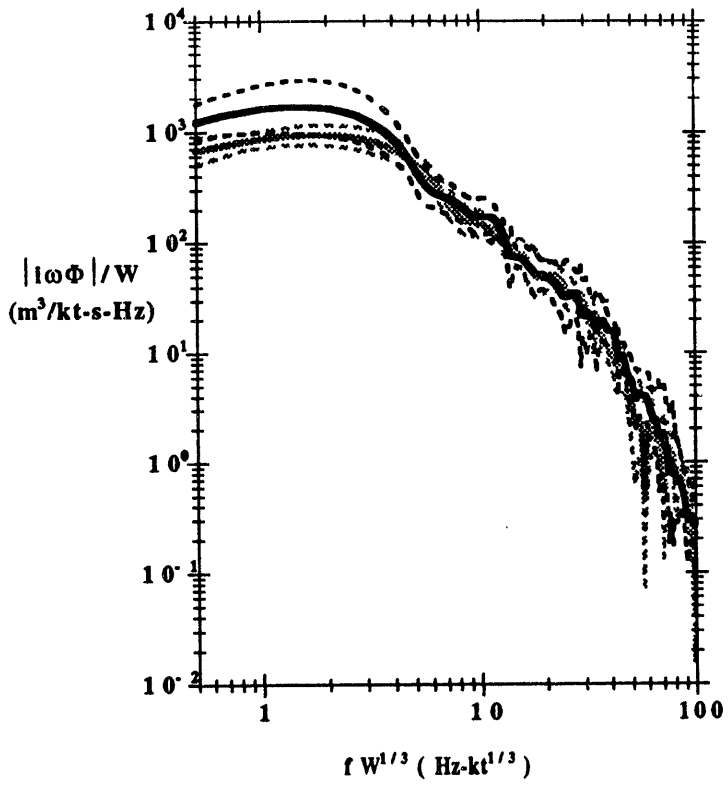

Fig. 2 Experimental free-field spectra. The solid curves are lognormal means, black for the NPE and gray for a nearby nuclear event. Dashed curves show ± 1 standard deviation.

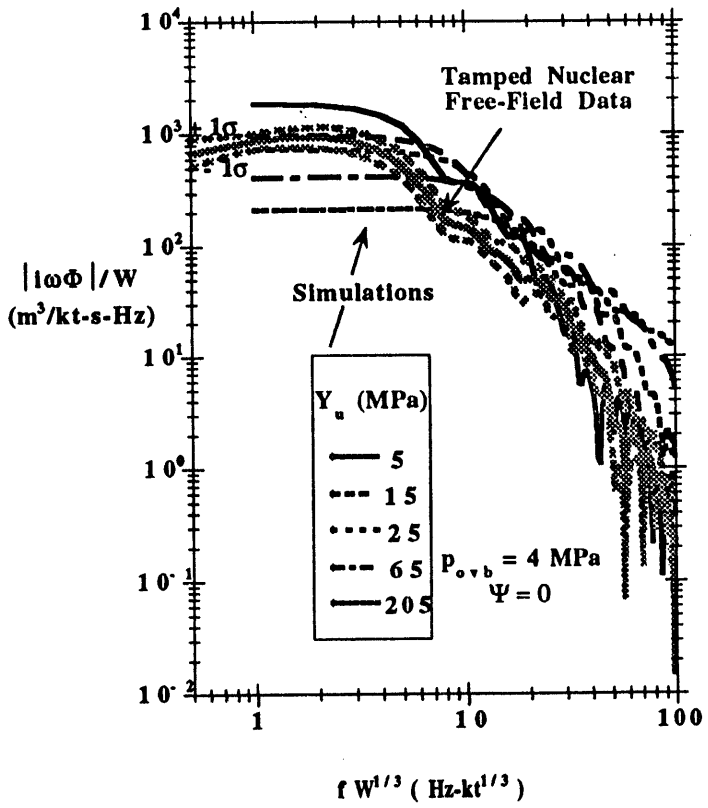

Fig. 3 Effect of varying the ultimate yield strength on seismic spectra. The corner frequency in the experimental data is best matched by the simulation with Y_u = 5 MPa

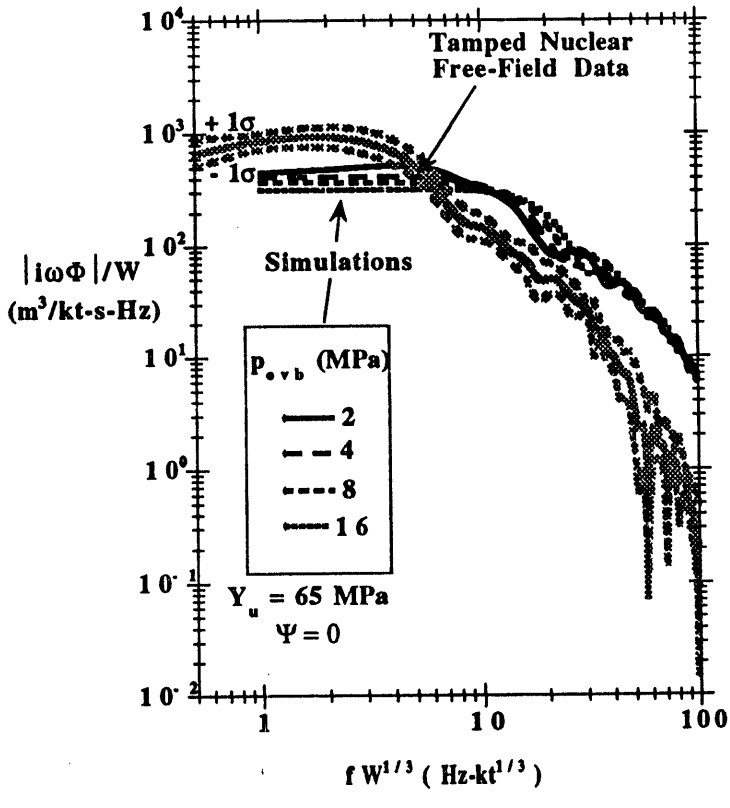

Fig. 4 Effect of varying the overburden pressure on seismic spectra. The corner frequency is relatively unaffected by changes in p_{ovb}.

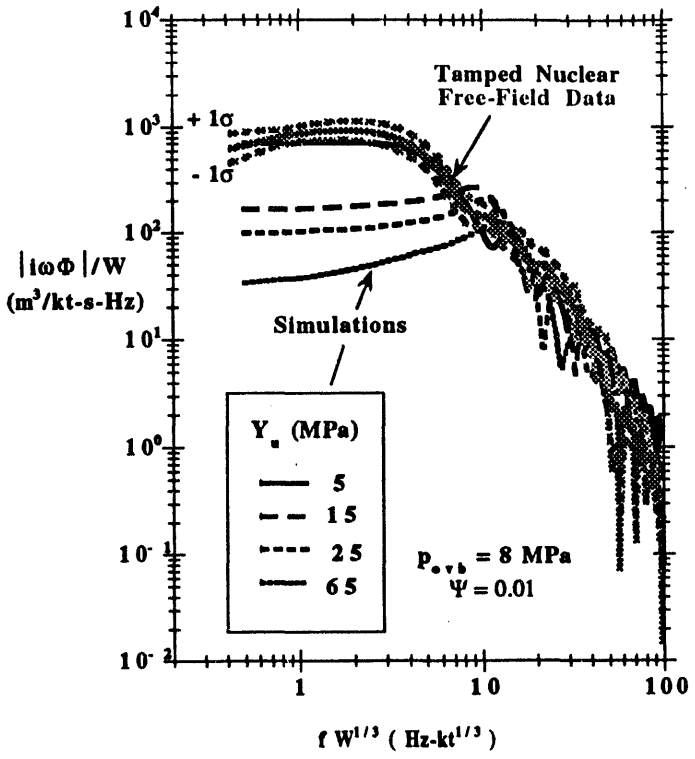

Fig. 5 Effect of varying the ultimate strength with $\Psi = .01$ & $p_{ovb} = 8$ MPa. The corner frequency in the experimental data is best matched by the simulation with $Y_u = 5$ MPa.

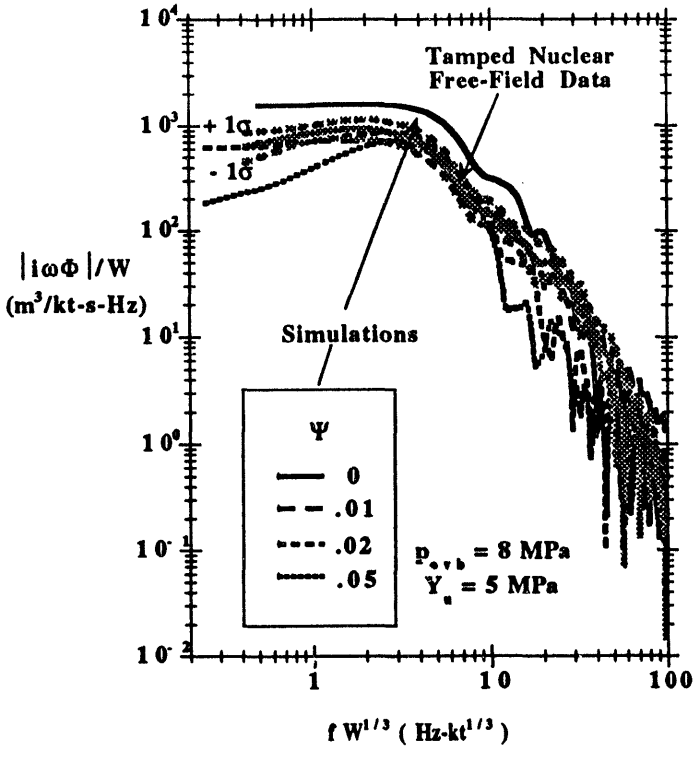

Fig. 6 Effect of varying the gas porosity with $Y_u = 5$ MPa & $p_{ovb} = 8$ MPa. The corner frequency is nearly independent of Ψ & the best fit to the experimental data is obtained with $0 < \Psi < 0.01$.

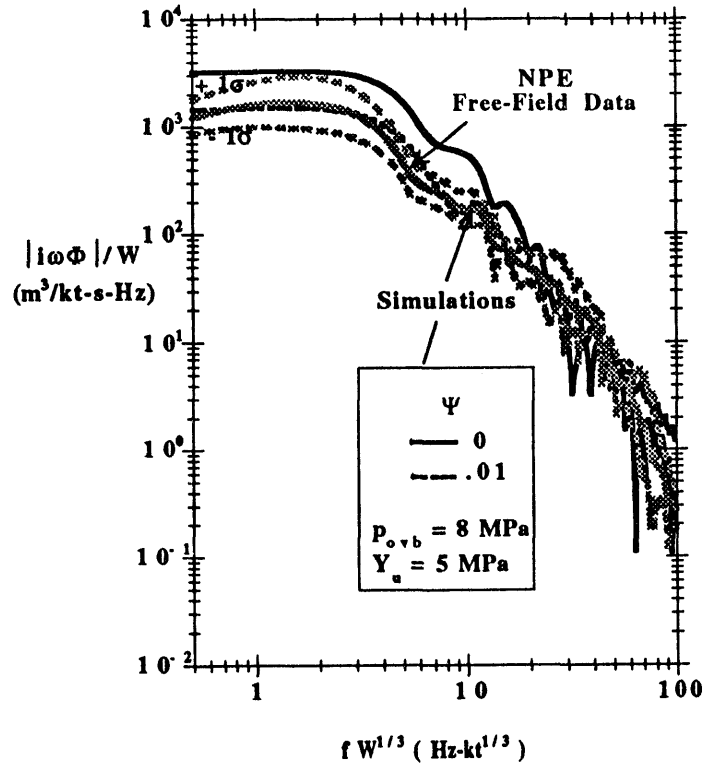

Fig. 7 Simulations of the NPE, with $0 < \Psi < 0.01$, $Y_u = 5$ MPa & $p_{ovb} = 8$ MPa. This parameter set is in good agreement with the experimental data for both the NPE and the nearby nuclear event (see Fig. 6).

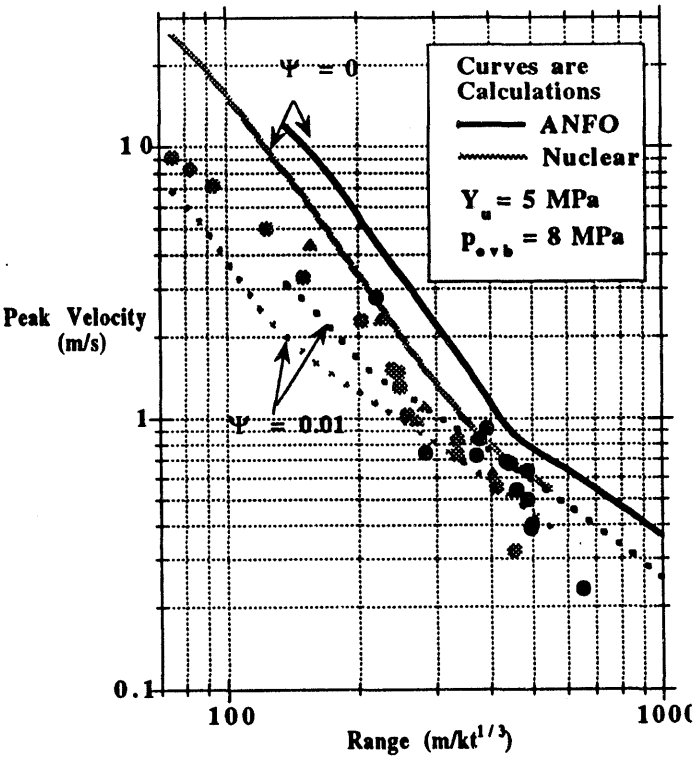

Fig. 8 Peak particle velocity as a function of range. Black dots are experimental data from the NPE and gray dots from nearby nuclear events.

Doc I

DATE FILMED

8/18/94

END